Magnetic Resonance Imaging 63 (2019) 159–169

Contents lists available at ScienceDirect

Magnetic Resonance Imaging

journal homepage: www.elsevier.com/locate/mri

Original contribution

Free-running simultaneous myocardial T1/T2 mapping and cine imaging with 3D whole-heart coverage and isotropic spatial resolution

Haikun Qi[a,*], Aurelien Bustin[a], Gastao Cruz[a], Olivier Jaubert[a], Huijun Chen[b], René M. Botnar[a,c], Claudia Prieto[a,c]

[a] School of Biomedical Engineering and Imaging Sciences, King's College London, London, United Kingdom
[b] Center for Biomedical Imaging Research, Department of Biomedical Engineering, Tsinghua University, Beijing, China
[c] Escuela de Ingeniería, Pontificia Universidad Católica de Chile, Santiago, Chile

ARTICLE INFO

Keywords:
Myocardial T1 mapping
Myocardial T2 mapping
Cine imaging
3D radial
Joint T1/T2

ABSTRACT

Purpose: To develop a free-running framework for 3D isotropic simultaneous myocardial T1/T2 mapping and cine imaging.

Methods: Continuous data acquisition with 3D golden angle radial trajectory is used in conjunction with T2 preparation of varying echo times and inversion recovery (IR) pulses to enable simultaneous myocardial T1/T2 mapping and cine imaging. Data acquisition is retrospectively synchronized with ECG signal, and 1D respiratory self-navigation signal is extracted from the k-space center of all radial spokes. Respiratory binning is performed based on the estimated respiratory signal, enabling estimation and correction of 3D translational respiratory motion. Using high-dimensionality patch-based undersampled reconstruction with dictionary-based low-rank inversion, whole-heart T1/T2 maps and cine images can be generated with 2 mm isotropic spatial resolution. The proposed technique was validated in a standardised phantom and ten healthy subjects in comparison to conventional 2D imaging techniques.

Results: Phantom T1 and T2 measurements demonstrated good agreement with 2D spin echo techniques. Septal T1 estimated with the proposed technique (1185.6 ± 49.8 ms) was longer than with a conventional breath-hold 2D IR-prepared sequence (1044.3 ± 26.7 ms), whereas T2 measurements (47.6 ± 2.5 ms) were lower than a breath-hold 2D gradient spin echo sequence (52.0 ± 1.8 ms). Precision of the proposed 3D mapping was higher than conventional 2D mapping techniques. Ejection fraction measured with the proposed 3D approach (63.8 ± 6.8%) agreed well with conventional breath-held multi-slice 2D cine (62.3 ± 6.4%).

Conclusions: The proposed technique provides co-registered 3D T1/T2 maps and cine images with isotropic spatial resolution from a single free-breathing scan, thereby providing a promising imaging tool for whole-heart myocardial tissue characterization and functional evaluation.

1. Introduction

Cardiac magnetic resonance imaging provides a comprehensive cardiac examination, including anatomy visualization, ventricular function estimation and myocardial tissue characterization, and has been used to diagnose and monitor a wide range of cardiac diseases [1,2]. Cine imaging is the gold standard to quantify cardiac function and enables cardiac wall motion assessment [3]. Parametric mapping of T1 and T2 times provides myocardial tissue characterization, notably manifesting fibrosis, edema and inflammation [4–8]. To measure cardiac function and tissue characterization clinically, separate 2D scans are usually performed sequentially under several breath-holds, suffering from limited coverage, moderate spatial resolution, complex scan planning, misregistration of different scans and patient fatigue. In contrast, simultaneous 3D myocardial T1/T2 mapping and cine imaging in a single free-breathing scan would simplify the imaging procedure and image analysis, providing comprehensive cardiac evaluation. In addition, co-registered myocardial T1 and T2 maps obtained in a single scan has potential to improve sensitivity, specificity and reader confidence for early diagnosis and treatment monitoring of cardiac diseases [1,8].

Commonly used myocardial T1 and T2 mapping techniques [9–11] adopt inversion recovery (IR), saturation recovery (SR) or T2 preparation (T2prep) pulses to generate T1 or T2 contrasts, followed by single-

* Corresponding author at: 3rd Floor, Lambeth Wing, St Thomas' Hospital, Lambeth Palace Rd, London SE1 7EH, United Kingdom.
E-mail address: haikun.qi@kcl.ac.uk (H. Qi).

https://doi.org/10.1016/j.mri.2019.08.008
Received 1 July 2019; Received in revised form 10 August 2019; Accepted 15 August 2019

shot acquisition at diastolic cardiac phase. For parametric fitting, several images with different T1 or T2 contrasts are acquired over several cardiac cycles in a single breath-hold, limiting these approaches to 2D imaging. Free-breathing 3D mapping techniques have been introduced to achieve higher signal-to-noise ratio (SNR), whole-heart coverage and better characterization of the spatial distribution of diffuse disease [12–16]. However, the requirement of respiratory gating to minimise breathing motion artifacts leads to long and unpredictable scan times.

Recently, 3D joint myocardial T1/T2 mapping techniques have been proposed to obtain co-registered T1 and T2 maps. Kvernby et al. [17] used interleaved T2 and IR prepared acquisitions in a single breath-hold to achieve simultaneous T1 and T2 mapping. Free-breathing joint T1 and T2 mapping has been proposed using SR and T2 preparations with respiratory gating [18]. However, to achieve whole-heart coverage with acceptable acquisition time, these techniques acquire only a few short-axis slices with a thick slice thickness (> 10 mm), and cardiac triggering is required for diastolic acquisition, resulting in scans with low acquisition efficiency.

Techniques for simultaneous T1 mapping and cine imaging have been proposed to improve acquisition efficiency, where continuous data acquisition is performed and T1 maps and cine images are reconstructed from the same scan [19,20]. In addition, magnetic resonance multitasking has shown great potential for motion-resolved quantitative myocardial T1 and T2 imaging from continuous 2D radial acquisition [21,22]. Although very promising, these techniques are still limited to 2D imaging, which are subject to insufficient coverage and through-plane motion.

A free-running 3D whole-heart myocardial T1 mapping technique allowing for T1 mapping for multiple cardiac phases with isotropic spatial resolution has recently been proposed [23]. Here we propose to extend this approach to enable simultaneous 3D myocardial T1/T2 mapping and cine imaging with whole-heart coverage and isotropic resolution from a single free-breathing scan. This is achieved by combining a continuous 3D golden angle radial acquisition with T2 preparation of varying echo times and IR pulses which generate different T1 and T2 contrasts. Joint T1/T2 mapping is performed for a given cardiac phase using the different T1/T2 contrasts, whereas 3D cine images can be obtained by reconstructing all cardiac phases with one contrast per cardiac phase. To reconstruct the highly undersampled 3D radial data after retrospective cardiac binning, a novel high-dimensionality patch-based undersampled reconstruction (HD-PROST) algorithm [24] is employed in concert with dictionary-based low-rank inversion [25].

The proposed technique was validated in a standardised T1/T2 phantom and in ten healthy subjects against conventional 2D techniques. The proposed 3D joint T1/T2 maps were compared with the 2D T1 and T2 maps obtained with a modified Look-Locker inversion recovery (MOLLI) [9] and a gradient spin echo (GraSE) [26] technique, respectively. Functional analysis obtained with the proposed 3D cine images was compared to a conventional breath-hold 2D multi-slice cine scan.

2. Methods

2.1. Free-running whole-heart multi-contrast imaging framework

2.1.1. Sequence design

The diagram of the proposed sequence is shown in Fig. 1A. The continuous acquisition is performed with a 3D golden angle radial sampling [23,27] to ensure pseudo-uniform distribution of radial spokes in the respiratory and cardiac bins, which are assigned retrospectively. Interleaved IR and T2prep pulses are employed to generate T1 and T2 contrasts. IR preparation only is performed for the first shot, whereas T2prep-IR pulses with two different T2prep echo times are performed in the following two shots. The 3-shot preparation pattern is repeated throughout the entire acquisition. To improve robustness to B0 and B1 inhomogeneities, the T2prep pulse is performed with two adiabatic refocusing pulses [28]. Following magnetization preparation, data acquisition is performed with low flip angle spoiled gradient-echo (SPGR) readout and a second order binomial (1-2-1) water-selective excitation pulse for fat suppression.

2.1.2. Motion extraction

Cardiac and respiratory motion signals are required for retrospective data binning. ECG time stamps are recorded and synchronized with data acquisition to determine the cardiac delay time for each radial spoke. The multi-coil k-space center of all radial spokes is employed to extract the signal component that is most relevant to the 1D superior-inferior respiratory motion using independent component analysis. Example of the extracted independent components and the self-navigated motion signal are provided in Supplemental Fig. S1. Details of the respiratory motion extraction can be found in [23].

2.1.3. Retrospective data binning

Based on the respiratory motion signal, the whole k-space data is binned into 5 equally populated respiratory phases from end-inspiration to end-expiration. According to the cardiac motion signal, the data at diastole is selected for each respiratory bin, from which 3D low-resolution diastolic images are reconstructed for each respiratory phase by using self-calibrating GRAPPA operator gridding [29]. Example short-axis images of the 5 respiratory phases are shown in Supplemental Fig. S2. By rigid registration of the heart region in the low-resolution diastolic images to that in the reference bin of end-expiration, the 3D translational respiratory motion parameters can be estimated and used to correct the corresponding k-space phase. The respiratory motion corrected k-space data can be binned into multiple cardiac phases according to the cardiac delay (cardiac binning), with each cardiac phase containing spokes of different inversion recovery times (TI) and T2prep durations, and thus different T1/T2 contrasts.

2.1.4. HD-PROST algorithm

After 3D translational motion correction and cardiac binning, the dictionary-based low-rank inversion algorithm is adopted to efficiently compress the T1/T2 contrasts to a few representative singular images [25] for joint T1/T2 mapping and cine reconstruction (details are given in the 2.3 Image reconstruction section). The recently proposed HD-RPOST algorithm [24] is utilized to reconstruct the highly undersampled data binned into a specific cardiac phase. The HD-PROST with dictionary-based low-rank compression is formulated as the following unconstrained Lagrangian [24]:

$$L(I, \mathscr{T}_p, Y) = \|EI - \sqrt{D}\,K\|_F^2 + \lambda \sum_p \|\mathscr{T}_p\|_* + \mu \sum_p \|\mathscr{T}_p - P_p(I) - P_p(Y)\|_F^2 \quad (1)$$

where I are the singular images to be reconstructed which are compressed from the T1/T2 image series; the encoding operator $E = \sqrt{D}F_{nu}U_r S$, with S being the sensitivity maps, U_r being the low-rank operator obtained by truncating the singular value decomposition (SVD) of the simulated dictionary (details given in the 2.3 Image reconstruction section), F_{nu} being the non-uniform Fast Fourier Transform (NUFFT), transforming Cartesian images to 3D radial k-space, and D being the non-Cartesian density compensation function; K is the undersampled k-space; $P_p(\cdot)$ is the patch selection operator, centered at pixel p of a 3D image set with multiple contrasts or single contrast. For single contrast (1 singular image to be reconstructed), this operator selects patches on a non-local (similar patches within a neighbourhood) scale, whereas in a multi-contrast setting, similar patches from all the contrasts are also selected [24]. $\mathscr{T}_p$ is a 3D tensor made of all the selected patches centered at pixel p by patch vectorization and concatenation; Y is the Augmented Lagrangian multiplier; λ is the sparsity-promoting regularization parameter and μ is the penalty parameter; $\|\cdot\|_F$

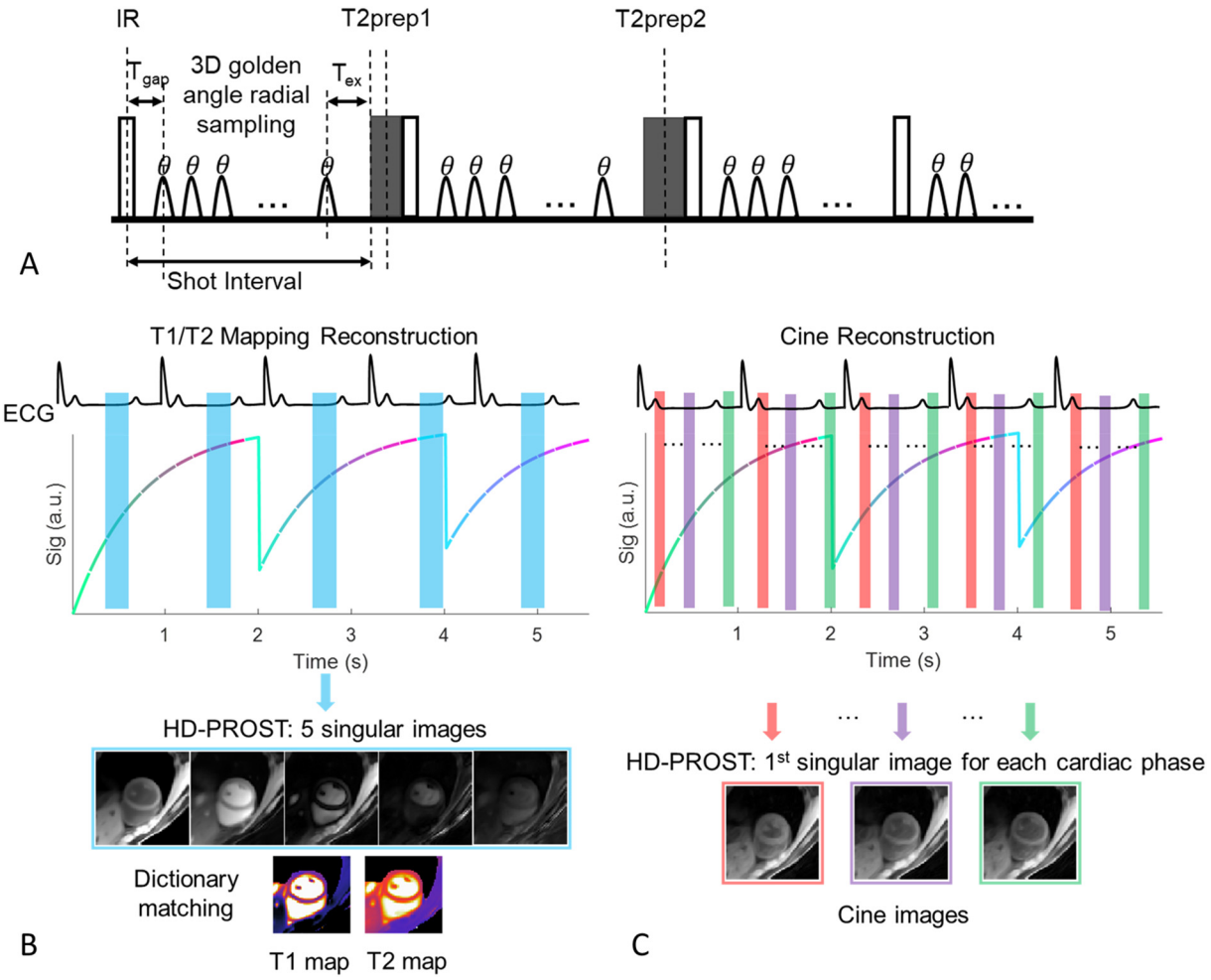

Fig. 1. A: Schematic diagram of the proposed free-running sequence, where 3 shots with different preparations are alternatively repeated throughout the scan. The first shot is only inversion recovery (IR) prepared, and T2 preparation with different echo times are added before IR in the next 2 shots. After preparation, spoiled gradient echo readout with low flip angle is performed using 3D golden angle radial trajectory. The shot interval is the time between the IR pulse and the start of the next preparation. T_{gap} is the time between the IR pulse and the first excitation and T_{ex} is the time interval between the last excitation and the start of the next preparation pulse. B: Joint T1/T2 mapping reconstruction: data at diastolic phase is selected, containing radial spokes of different T1/T2 contrasts, from which 5 singular images are reconstructed with HD-PROST. Dot product dictionary matching between the measured and simulated signal is performed to generate T1 and T2 maps. C: Cine reconstruction: k-space is binned into 16 cardiac phases. The first singular image with the highest signal-to-noise ratio is reconstructed with HD-PROST for each cardiac phase.

and $\|\cdot\|_*$ denote the Frobenius norm and nuclear norm respectively. The reconstruction Eq. (1) can be efficiently solved by operator-splitting via alternating direction method of multipliers (ADMM). Further details of the reconstruction algorithm can be found in [24].

2.2. Data acquisition

The proposed framework was tested in phantom and in vivo imaging on a 1.5 T MRI scanner (Ingenia, Philips Healthcare, Best, the Netherlands) using a 28-channel cardiac coil. The following scan parameters were used for the proposed sequence: FOV = $200\times200\times200\text{mm}^3$ (with 2-fold readout oversampling, the acquired FOV = $400\times400\times400\text{mm}^3$); spatial resolution = $2\times2\times2\text{mm}^3$; TR/TE = 10.3 ms/4.6 ms; flip angle = 6°; T2prep echo times = [30,60]ms; T_{gap} (Fig. 1A) = 9.5 ms (minimum values allowed on the scanner); shot interval (Fig. 1A) = 2200 ms; number of readouts after preparation = 195, resulting in T_{ex} (Fig. 1A) = 182 ms for signal recovery.

2.2.1. Phantom imaging

A standardised T1/T2 phantom [30] consisting of 9 agarose-based vials with T1 values ranging from 250 ms to 1600 ms and T2 values ranging from 40 ms to 230 ms was imaged to compare T1, T2 measurements between the reference spin echo methods, and 2D T1 MOLLI, 2D T2 GraSE and the proposed 3D free-running sequence. Reference T1 values were obtained using the 2D inversion recovery spin echo (IR-SE) sequence with the following imaging parameters: FOV = $140\times140\text{ mm}^2$; in-plane spatial resolution = $1.5\times1.5\text{mm}^2$; slice thickness = 8 mm; TR/TE = 10,000/5.8 ms; 13 TIs = [50, 100, 200, 300, 400, 500, 700, 900, 1200, 1500, 2000, 2500, 3000] ms. The 2D multi-echo spin echo (ME-SE) was performed for reference T2 measurement with the same FOV and spatial resolution as 2D IR-SE. Additional imaging parameters were: TR = 15,000 ms, 8 TE values from 10 ms to 80 ms with an interval of 10 ms. Standard T1 and T2 values were determined by non-linear least-squares fitting with a 3-parameter IR model for T1 and a 2-parameter T2 decay model for T2.

The 2D MOLLI (3-3-5) [31] imaging parameters were: TR/TE = 2.6/1.3 ms; flip angle = 35°; FOV = $288\times288\text{ mm}^2$; in-plane resolution = $2\times2\text{ mm}^2$; slice thickness = 8 mm; diastolic acquisition window = 187 ms. The 2D GraSE sequence [26] was performed with the same FOV and spatial resolution to MOLLI, and other parameters were: turbo spin echo factor (number of multi-echo images) = 9; echo-

planar-imaging readout factor = 7; TR = 1 heart beat; ΔTE = 8.8 ms; flip angle = 90°; double inversion recovery black-blood prepulse. MOLLI and GraSE were acquired with simulated heart rate of 60 bpm and parallel imaging acceleration factor of 2. The 2D T1 and T2 maps were obtained with the vendor software package by fitting the 3-parameter model for MOLLI images [31] and the T2 decay model for GraSE images [26].

For the proposed 3D free-running sequence, the ECG signal was simulated with heart rate varying between 50 bpm and 70 bpm. The acquired 3D radial data was retrospectively binned for a simulated diastolic phase containing a series of T1/T2 contrasts. Then, 3D T1 and T2 phantom images were reconstructed using HD-PROST. More details for the joint T1/T2 mapping reconstruction are given in the following Image reconstruction section.

2.2.2. In vivo imaging

Ten healthy subjects (6 females; age: 32.6 ± 3.7 years) were recruited in this study with approval from the local institutional review board and written informed consent from all the subjects before imaging. A conventional 2D cine cardiac MRI was performed in the mid-ventricular short-axis plane with a short breath-hold of 2.6 s and retrospective gating of 16 cardiac phases, from which the diastolic cardiac delay was determined for each subject. Following the 2D cine scan, 2D mapping acquisitions including T1 MOLLI and T2 GraSE were performed in the same mid short-axis view at diastole with the same imaging parameters as the phantom study.

For cardiac function measurement reference, conventional breath-held 2D multi-slice and retrospective ECG-gated cine MRI was performed in the short-axis orientation covering the entire left ventricle. Imaging parameters included: FOV = $320 \times 320\ mm^2$, spatial resolution = $2 \times 2\ mm^2$, slice thickness = 8 mm, 12 slices, TR/TE = 3.0/1.5 ms, flip angle = 60°, retrospective gating to 20 cardiac phases. With parallel imaging acceleration factor of 2, the entire acquisition required 4 breath-holds with 3 slices acquired per breath-hold of about 13 s. The breath-hold 2D multi-slice cine data was acquired on 7 subjects of the 10 participants.

The proposed free-breathing 3D sequence was performed on all subjects with the same imaging parameters as the phantom study. Total scan time was 11.2 min, resulting in an acquisition with 300 shots (58,500 radial spokes).

2.3. Image reconstruction

2.3.1. Joint T1/T2 mapping reconstruction

For comparison with conventional 2D mapping methods, diastolic 3D T1 and T2 maps were reconstructed with the proposed approach. As shown in Fig. 1B, retrospective binning was performed for diastolic phase with acquisition window similar to the 2D MOLLI scan (~187 ms). Based on the TI and T2prep echo times, the spokes binned to diastole were sorted into 30 T1/T2 frames with temporal window width of about 196 ms along the contrast dimension. Then, a dictionary-based low-rank compression was performed along the contrast dimension to exploit the redundancy of the 30 T1/T2 frames and to further reduce the number of contrasts to be reconstructed with HD-PROST to save computation memory and time. The dictionary used for low-rank compression was simulated for T1 from 100 ms to 3000 ms and for T2 from 10 ms to 300 ms with a linear increment of 1% for both T1 and T2. The dictionary was simulated according to the spokes binned into the diastolic cardiac phase, and the signal of each radial spoke was calculated using Bloch equation (details of adopted signal equations are provided in the Supplemental File). SVD of the dictionary gives the singular values and singular vectors, and the low-rank operator U_r in the reconstruction equation was obtained by keeping the 5 largest singular vectors.

For HD-PROST reconstruction [32], the following parameters were used: patch size = $5 \times 5 \times 5$; search window = $10 \times 10 \times 10$; patch offset = 3; number of selected similar patches = 20; regularization parameters $\lambda = 0.015$, $\mu = 0.01$, which were empirically optimized by visual inspection of the reconstructed image quality in a subset of datasets and kept constant for all reconstructions.

2.3.2. Myocardial T1/T2 and blood T1 estimation

After HD-PROST reconstruction, 5 singular images were obtained. The dot product dictionary matching was performed on the singular images to generate T1 and T2 maps (Fig. 1B), where myocardial T1 and T2 values were extracted. T1 in the blood pool may be useful for extracellular volume measurement. However, the signal model (Supplemental File) used for myocardial T1 and T2 mapping is only valid for static tissue that experiences all the preparation and excitation pulses, which may not be true for flowing blood. To better model the mixing of inflow of fresh blood in the blood pool, the dictionary for blood was simulated by using a close to zero flip angle and zero T2prep echo times such that the blood magnetization was approximately unperturbed inversion recovery [22]. Then, a second dictionary matching was performed at the mid-ventricle short-axis location to obtain the T1 value in the left ventricle blood pool.

2.3.3. Cine reconstruction

For cine image reconstruction (Fig. 1C), the k-space data was binned into 16 cardiac phases with temporal resolution of ~60 ms. The radial spokes binned to one cardiac phase have different TI times, and thus have positive or negative signals. If mixed together for reconstruction, the signal cancelation will reduce the SNR of the reconstructed image. Therefore, based on spoke TI times, neglecting T2prep difference, the spokes binned to each cardiac phase were sorted into 4 TI frames with temporal window width of about 500 ms. Similar to the T1/T2 mapping reconstruction, a dictionary for low-rank compression was generated for each cardiac phase to exploit the contrast redundancy and the rank value was set to 1, which means only the first singular image with the highest SNR was reconstructed. The HD-PROST reconstruction [Eq. (1)] was repeated for all cardiac phases to obtain the cine images (Fig. 1C). Reconstruction parameters were the same as the HD-PROST joint T1/T2 mapping reconstruction, except that the number of selected similar patches was set to 10 and $\lambda = 0.03$.

2.4. Image analysis

2.4.1. Joint T1/T2 mapping

For the phantom study, circular region-of-interest (ROI) was defined for each vial and the mean and standard deviation (SD) of T1 and T2 values within the ROI were calculated. Using the T1, T2 measurements from the 2D IR-SE and ME-SE methods as references, the accuracy of T1 MOLLI, T2 GraSE and the proposed 3D joint T1/T2 mapping technique was evaluated by comparing the estimated T1, T2 values using linear correlation and Bland-Altman analyses.

For in vivo mapping analysis, 3 slices from base, mid and apex were selected to evaluate the spatial distribution of T1 and T2 in the 3D maps. Myocardial segments were defined according to the American Heart Association (AHA) standard [33], with 6 segments in the basal and mid slices and 4 segments in the apical slice. The T1 and T2 values of each myocardial segment were calculated by averaging across all the subjects and were visualized with bull's eye plots. To compare with the 2D breath-hold mapping methods, the mid short-axis slice from the 3D T1/T2 maps with the most similar geometry to MOLLI and GraSE maps was selected. ROIs were defined in the septum for MOLLI, GraSE and the proposed 3D T1/T2 mapping approach. To evaluate the in vivo T1 and T2 estimation accuracy and precision of the proposed 3D method, the mean and SD of T1 and T2 values within the septal ROI were calculated and compared with the conventional 2D methods using the Wilcoxon rank-sum test.

2.4.2. Cardiac function

End-systolic volume (ESV), end-diastolic volume (EDV), and ejection fraction (EF) were compared between the 3D cine images with the proposed method and the conventional breath-held 2D multi-slice cine images. A freely available software (http://medviso.com/segment/) [34] was used for ventricular segmentation and volume measurement. Segmentation was performed for the end-systolic and end-diastolic frames. For 2D cardiac cine images, the endocardial border of the left ventricle was segmented on all acquired slices. 3D cine images were reformatted to 12 short-axis slices with 8 mm thickness corresponding to the 2D cine slices before segmentation. After segmentation, the left ventricular volume was calculated according to the number of left ventricular voxels and the voxel volume. From EDV and ESV, the EF was calculated as $100 \cdot (EDV - ESV)/EDV$. Bland-Altman analysis was used to compare the cardiac function measurements of the proposed technique with the 2D multi-slice cine.

All image reconstructions, analysis and statistical analysis were performed using MATLAB (the MathWorks, Natick, MA, USA) on a server with a dual 16-core CPU, and 256GB RAM. A P value < 0.05 was considered statistically significant.

3. Results

3.1. Phantom experiments

Phantom T1 and T2 maps obtained with the 2D spin echo methods, MOLLI, GraSE and the proposed 3D approach are shown in Fig. 2A, where homogeneous T1 or T2 maps are observed for all the methods. The mean and SD of T1 and T2 values of each vial are compared in Fig. 2B. T1 estimations with the proposed method were in good agreement with the reference 2D IR-SE sequence, whereas, MOLLI severely underestimated long T1 values. For T2, the proposed approach showed better accuracy than GraSE for short and intermediate T_2 values (< 150 ms) in comparison with 2D ME-SE. However, underestimation of long T2 values was observed with the proposed 3D approach. The Bland-Altman plots in Fig. 3 compare the reference T1 values estimated by 2D IR-SE respectively with the proposed 3D and MOLLI methods, and the reference T2 values estimated by 2D ME-SE respectively with the proposed 3D and GraSE techniques. The percentage error of the T1 measurements was 2.1 ± 1.8% (0.4% - 5.5%) for the proposed approach and 7.1 ± 4.6% (0.2% - 13.6%) for MOLLI. The percentage error of the T2 measurements was 3.0 ± 4.0% (0.2% - 11.9%) for the proposed approach and 4.8 ± 1.8% (1.7% - 7.3%) for GraSE.

3.2. In vivo experiments

All images were reconstructed successfully with the proposed approach. The fully sampled number of spokes of the 3D radial acquisition with 200 mm isotropic FOV and 2 mm isotropic voxel size should be $100 \times 100 \times \pi/2 = 15{,}708$ according to the Nyquist rule. For diastolic T1/T2 mapping reconstruction, each T1/T2 frame may contain different number of spokes ranging from 120 to 500 spokes, resulting into acceleration factor of 30 to 130. For 16-cardiac phase cine reconstruction, the number of spokes binned into one cardiac phase is around 3500, leading to 4.5-fold acceleration. The reconstruction time was approximately 312 min for the 3D diastolic joint T1/T2 mapping, whereas, for 3D cine reconstruction, it took approximately 62 min per cardiac phase.

3.2.1. Joint T1/T2 mapping

3D T1 and T2 mapping results from a healthy subject, including 8 representative short-axis slices and a long-axis slice are shown in Fig. 4. Uniform spatial distribution of myocardium T1 and T2 over the entire left ventricle can be observed. T1 and T2 distributions across the left ventricle by the proposed technique for all subjects are shown in the bull's-eye plots in Fig. 5A. To better visualize the variability of T1 and T2 measurements over the left ventricle, box-plots of the T1 and T2 values of the 16 AHA segments are shown in Fig. 5B. As can be seen, inferior segments showed lower T1 values than other segments, especially in the apex slab. T2 distribution in the AHA segments was overall uniform, except for the septal segment in the apical slab that had higher T2 values.

Diastolic T1 and T2 mapping results from another 2 subjects are shown in Fig. 6, including the basal, mid and apical short-axis slices

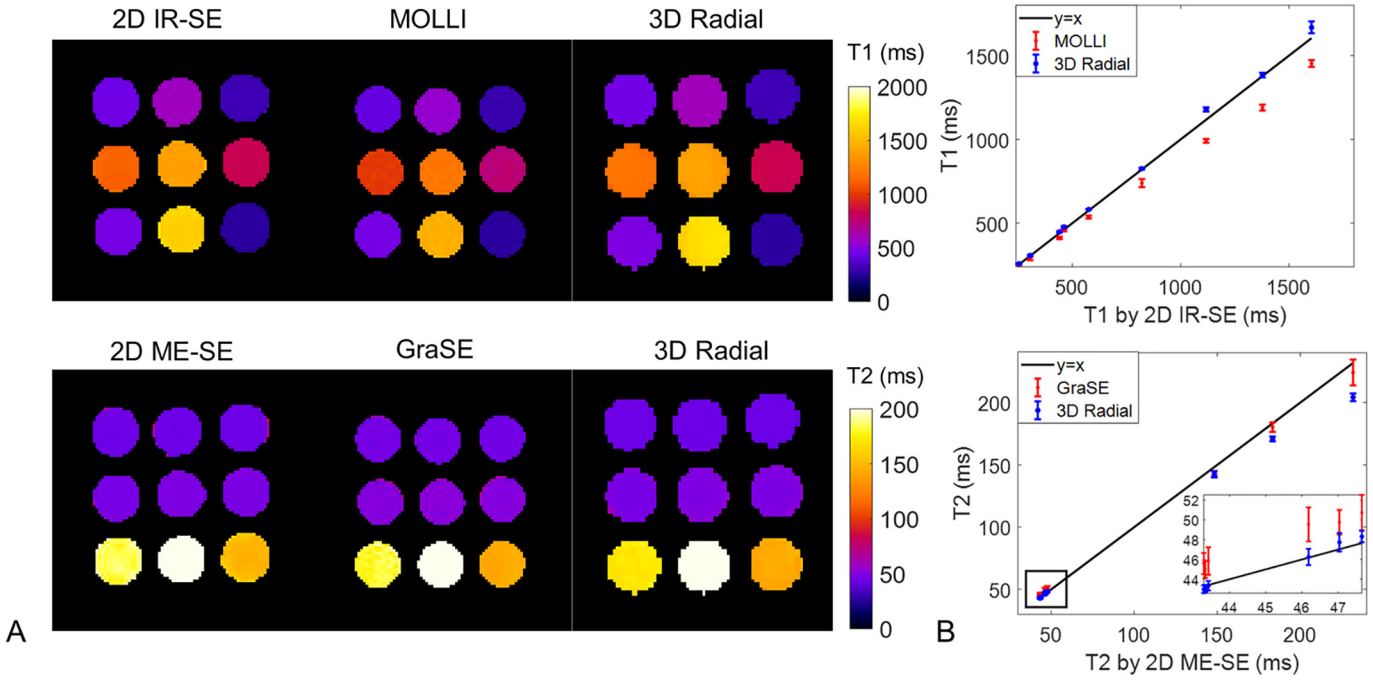

Fig. 2. A: Phantom T1 and T2 maps of 2D IR-SE, 2D ME-SE, T1 MOLLI, T2 GraSE and the proposed 3D joint T1/T2 mapping approach. B: Linear correlation of phantom T1, T2 estimations of MOLLI (y = 0.86x + 35.5, $R^2 = 0.99$), GraSE (y = 0.95x + 4.92, $R^2 = 0.99$) and the proposed 3D method (T1: y = 1.03x − 7.44, $R^2 = 0.99$; T2: y = 0.88x + 6.14, $R^2 = 0.99$) with the reference 2D spin echo methods.

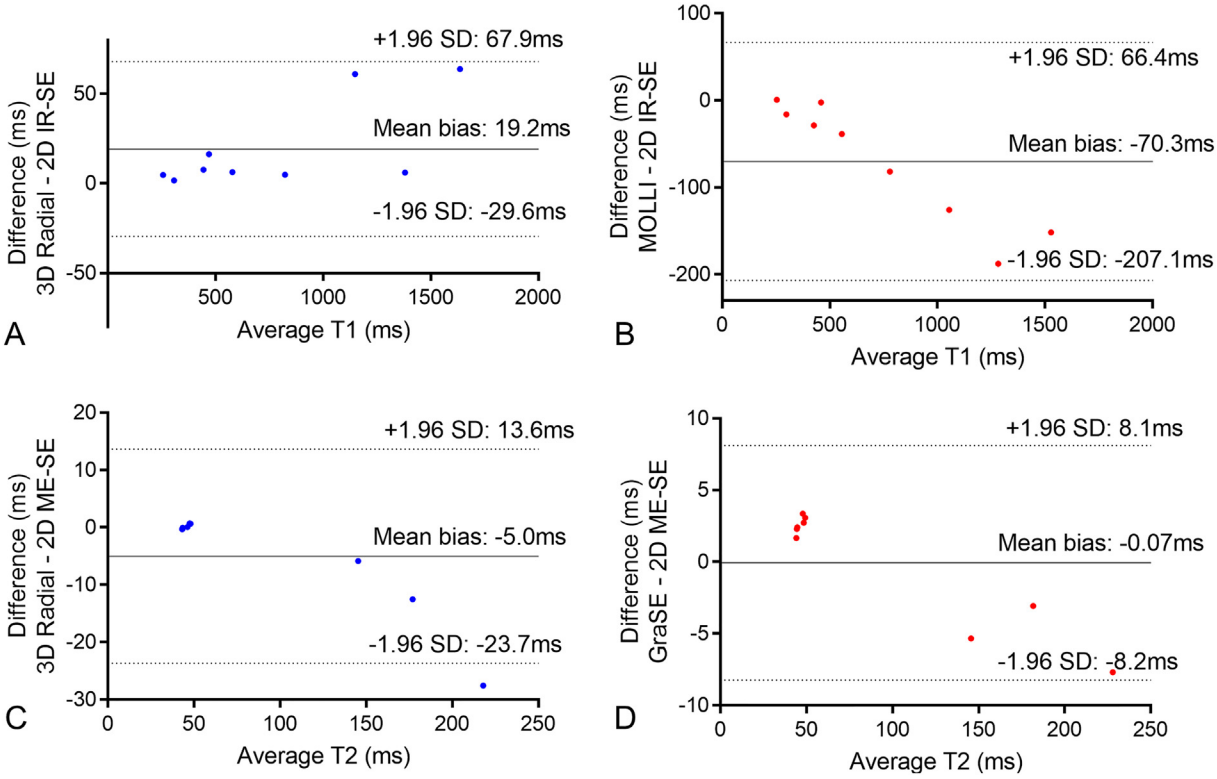

Fig. 3. Bland-Altman plots compare the reference T1 values estimated by 2D IR-SE respectively with the proposed 3D mapping (A) approach and MOLLI (B), and the reference T2 values estimated by 2D ME-SE respectively with the 3D method (C) and GraSE (D). The grey solid line indicates the mean difference, and the grey dotted lines indicate the 95% confidence intervals of limits of agreement.

from the 3D mapping approach and the mid short-axis slice from 2D MOLLI and GraSE. Mean and standard deviation of septal T1 and T2 values of all 10 subjects are compared between the proposed 3D technique, and MOLLI, GraSE in Fig. 7. Higher T1 (1185.6 ± 49.8 ms) and slightly lower T2 (47.6 ± 2.5 ms) values were obtained with the proposed method, compared with MOLLI (1044.3 ± 26.7 ms, $P < 0.01$) and GraSE (52.0 ± 1.8 ms; $P < 0.01$), which were in agreement with the phantom findings. The standard deviation of the T1 and T2 values in the septum was lower with the proposed 3D method (SD of T1: 29.4 ± 7.1 ms; SD of T2: 1.9 ± 0.6 ms) than the 2D methods (SD of MOLLI T1 46.9 ± 10.5 ms, $P < 0.01$; SD of GraSE T2 3.7 ± 1.5 ms; $P < 0.01$). Blood T1 estimated from the 3D acquisition was 1703.0 ± 90.8 ms, which was higher than that of MOLLI 1599.3 ± 87.1 ms.

3.2.2. *Cine function*

Besides joint 3D T1/T2 maps, 3D cine images can be reconstructed from the proposed free-running sequence. The cine images of the subject in Fig. 4 are shown in Fig. 8, where the short-axis and long axis slices corresponding to that of Fig. 4 are visualized both at systole and diastole. Comparison of the proposed 3D free-breathing cine images with breath-hold 2D multi-slice cine images from another two subjects is shown in Fig. 9. The 3D acquisition has isotropic resolution and can be reformatted to any arbitrary orientations, as evident by the long-axis view in Figs. 8, 9. ESV, EDV and EF measurements of the 7 subjects estimated from the proposed 3D technique and 2D multi-slice cine imaging are compared in Fig. 10A. Bland-Altman analysis (Fig. 10B) suggests good agreement of the two methods for cardiac function quantification.

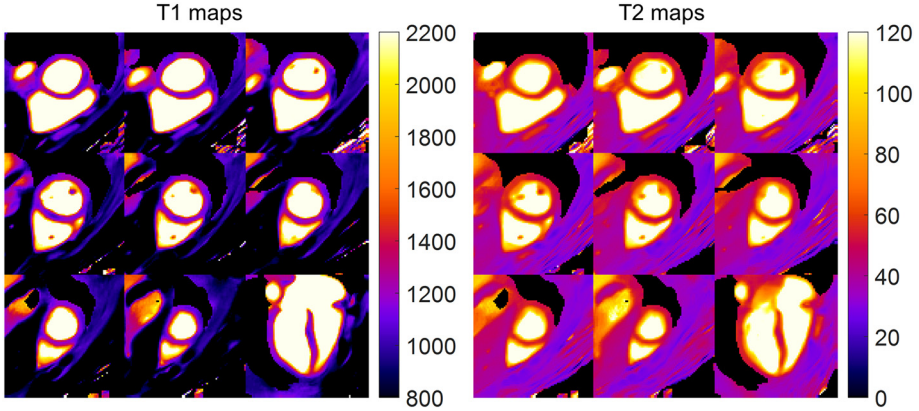

Fig. 4. T1 and T2 mapping results from a representative healthy subject using the proposed 3D free-running technique. Eight short-axis slices, from base to apex of the left ventricle including the long-axis view are shown. Uniform T1 and T2 distributions across the left ventricle can be observed.

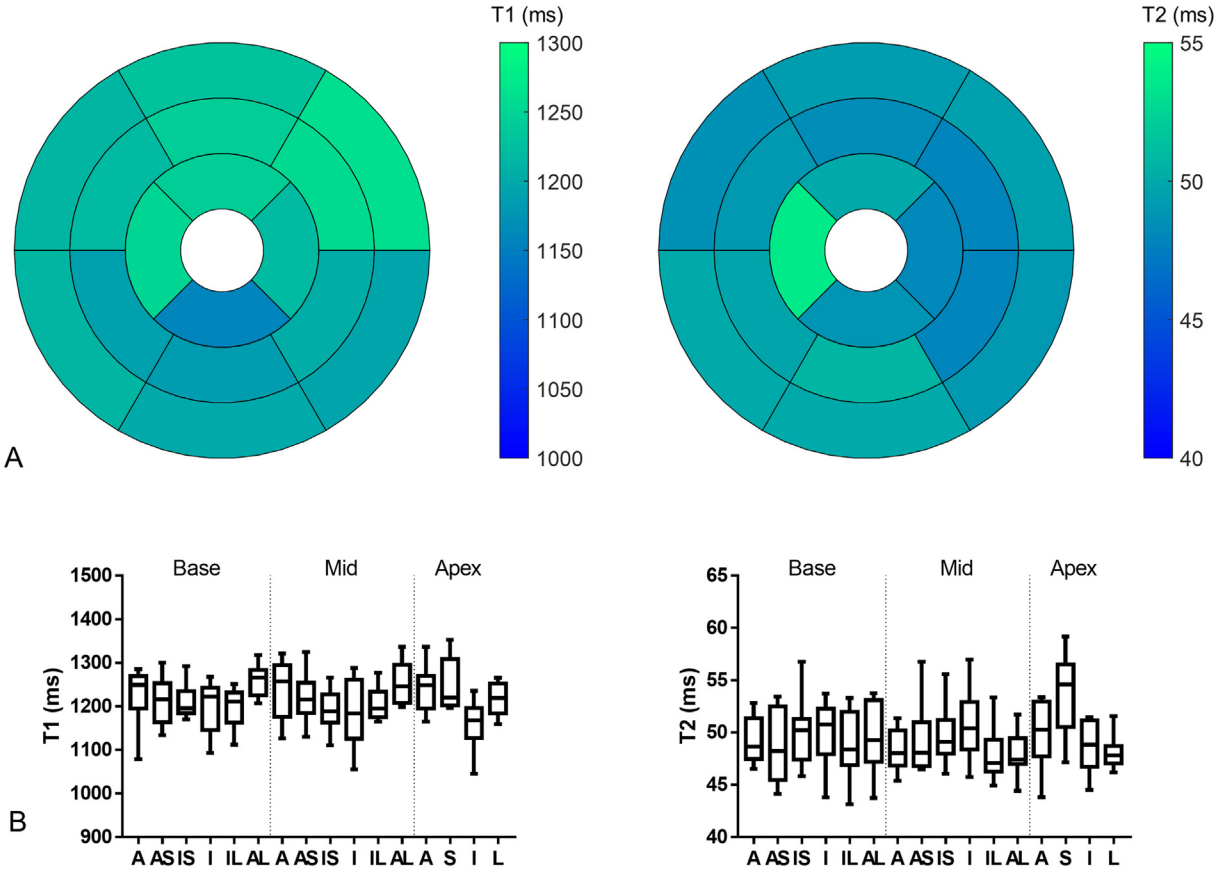

Fig. 5. A: AHA bull's eye plots showing the myocardium T1 and T2 distributions across the left ventricle with the proposed joint 3D T1/T2 mapping technique averaged for all healthy subjects. B: Box plots showing the median, 25 and 75 percentiles, and range of T1 and T2 values in each AHA segment from all the subjects. (A: anterior; AS: anteroseptal; IS: inferoseptal; I: inferior; IL: inferolateral; AL: anterolateral; S: septal; L: lateral).

4. Discussion

In this study, a free-running (free-breathing, retrospective cardiac binning) framework was proposed for simultaneous 3D myocardial T1/T2 mapping and cine imaging with whole-heart coverage and isotropic spatial resolution. This sequence used IR and T2 preparations to introduce T1 and T2 contrasts and a 3D golden angle radial trajectory for continuous data acquisition allowing for flexible retrospective respiratory and cardiac binning. Using high-dimensionality patch-based undersampled reconstruction [24] with dictionary-based low-rank inversion [25], whole-heart T1 and T2 maps and cine images are generated with 2 mm isotropic spatial resolution from a ~11 min single scan. Phantom results showed that the proposed approach achieves good accuracy and precision compared with 2D IR-SE and 2D ME-SE references. Co-registered 3D T1 and T2 maps and cine images of 16 cardiac phases were demonstrated in vivo. Myocardial T1 and T2 measurements with the proposed 3D technique were comparable to conventional breath-hold, cardiac-triggered 2D MOLLI and GraSE. Measurements of ESV, EDV and EF for cardiac function assessment were in good agreement with conventional breath-hold 2D multi-slice cine

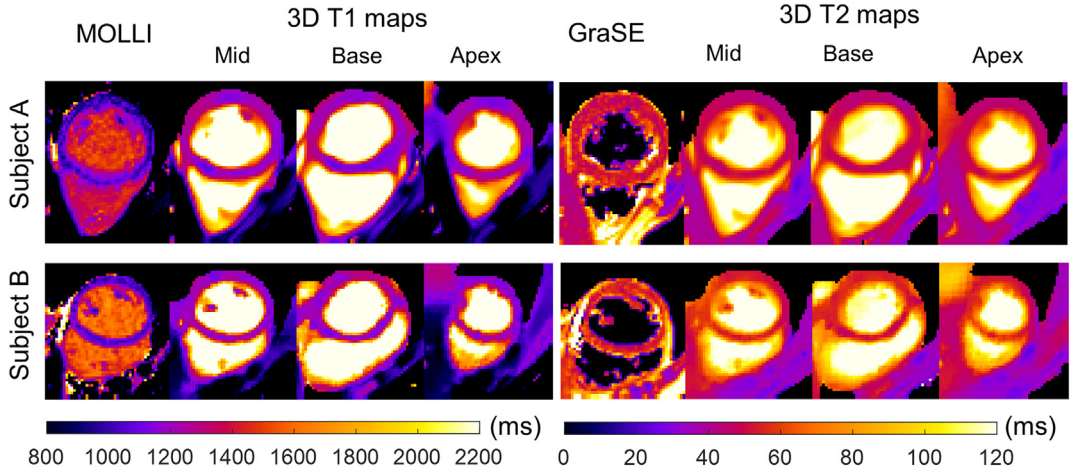

Fig. 6. Short-axis 2D MOLLI, 2D GraSE and the proposed 3D joint T1/T2 mapping results for two healthy subjects. Representative basal and apical slices from the proposed 3D approach are also shown for each subject.

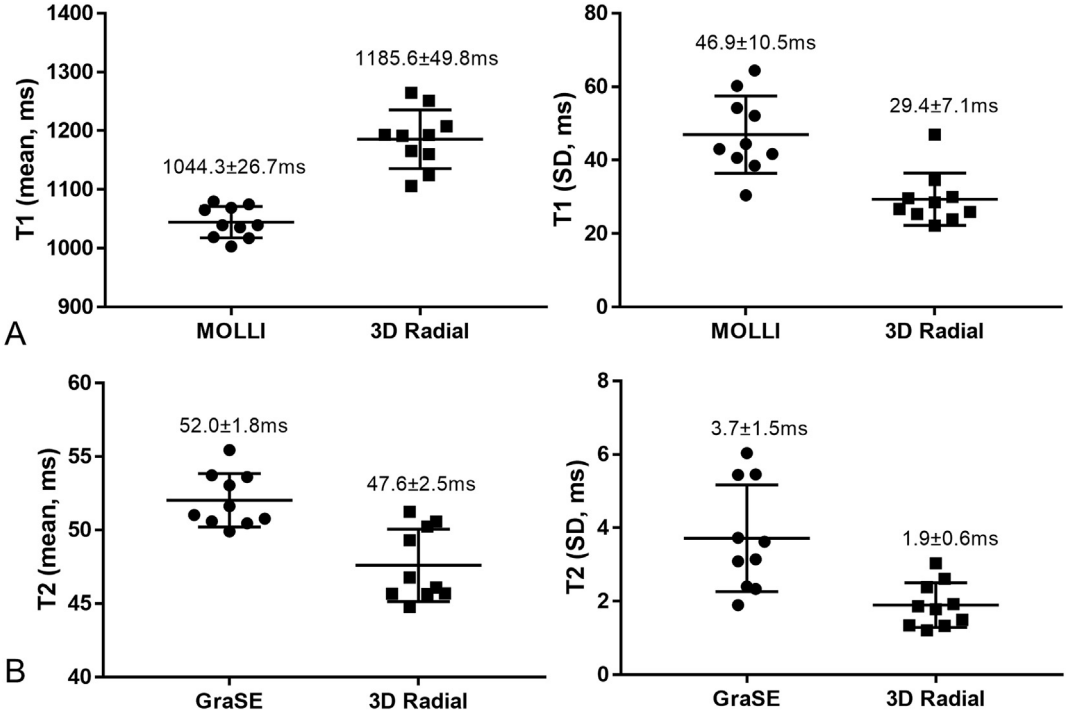

Fig. 7. Mean and standard deviations of septum T1 (A) and T2 (B) values for all 10 healthy subjects measured with 2D MOLLI, 2D GraSE and the proposed 3D joint T1/T2 mapping technique.

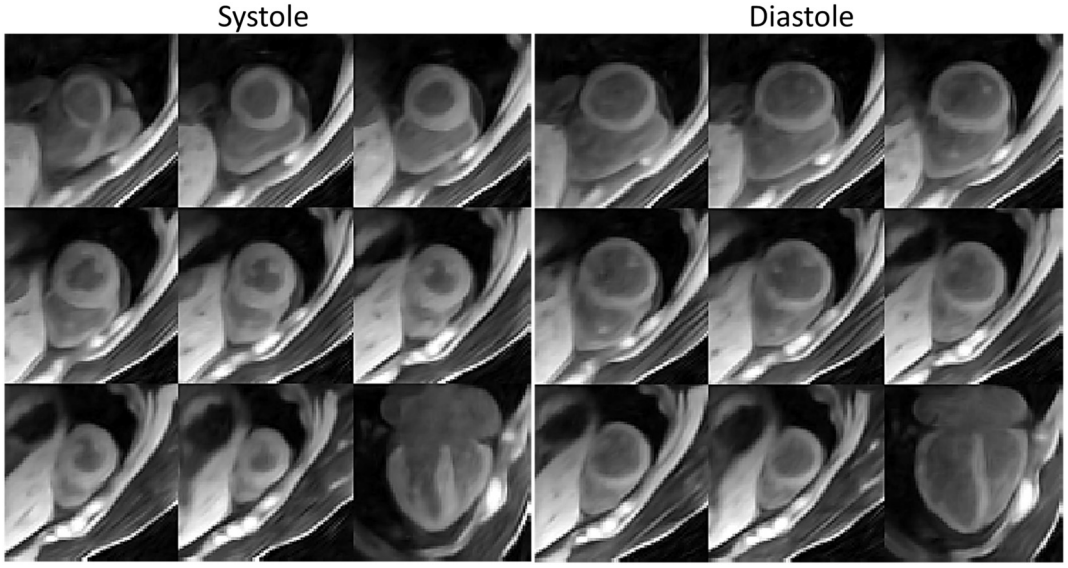

Fig. 8. Reconstructed 3D cine images at systole and diastole for the subject shown in Fig. 4, including 8 short-axis slices from base to apex and the long-axis view.

images.

In the phantom study, the proposed 3D technique achieved better accuracy than 2D MOLLI for T1 measurements in the range of 250 ms to 1600 ms. As expected, MOLLI underestimated longer T1 values partly due to the incomplete longitudinal magnetization recovery for long T1 which violates the MOLLI assumption of full recovery before the next IR [9]. Compared with T2 GraSE, similar or better T2 estimation accuracy was achieved with the proposed 3D approach in the T2 range of 40 ms to 150 ms. For longer T2 (150-230ms), GraSE showed better accuracy than the proposed approach although with higher measurement variability. For measuring myocardial T2, the proposed sequence adopted a longest T2prep echo time of 60 ms. However, this T2prep echo time may not be long enough to accurately quantify longer T2 values. Increasing the T2prep echo times could improve the accuracy for larger T2 values, however, at the cost of a reduction in SNR.

The in vivo myocardial T1 and T2 measurements were in agreement with the phantom findings. Compared with MOLLI, the proposed technique resulted in significantly longer septal T1 values. The septal T2 values measured with the proposed 3D technique were slightly shorter than those measured with GraSE. Compared with 2D methods, the proposed 3D method showed lower SD of T1 and T2 measurements in the septum. This may be due to the 3D nature of the acquisition which help minimising the 2D imaging limitations of low SNR and through-plane motion artifacts. Also, the adopted HD-PROST denoising reconstruction may help to further reduce the measurement SD [24]. Moreover, the proposed acquisition uses low flip angle SPGR readout,

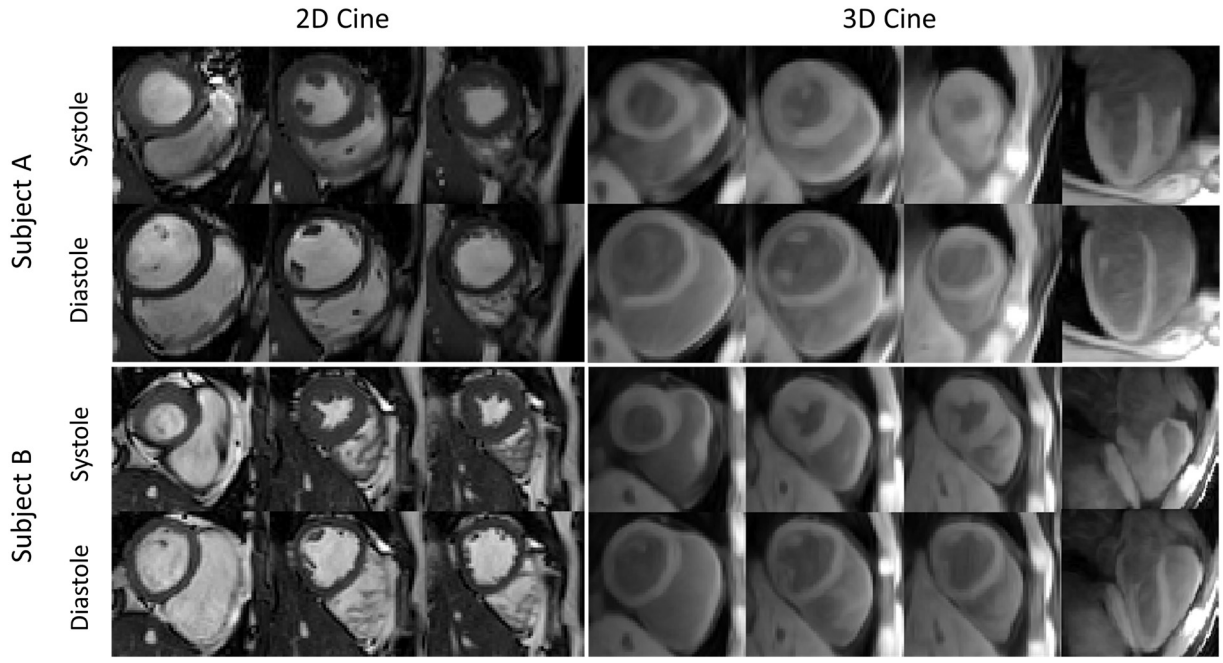

Fig. 9. Comparison of the breath-hold 2D multi-slice cine and the proposed 3D cine at systole and diastole for two subjects. Three short-axis slices from basal, mid and apical left ventricle are shown for both methods. The reconstructed 3D cine images have isotropic resolution, and the long-axis view can be reformatted which is shown in the last column.

which is less sensitive to field inhomogeneities than bSSFP, and radial sampling trajectory that is intrinsically less sensitive to motion than Cartesian sampling. These advantages make the proposed 3D free-running technique a promising tool for whole-heart joint T1/T2 mapping.

The 16-segment AHA analysis revealed small fluctuations of T1 and T2 values between different segments. Shorter T1 values measured in the inferior segments may be attributed to residual respiratory motion, which is consistent with results reported in previous studies [16,18]. When defining the myocardium contour, more partial volume effects from blood were observed for the septal segment of apex, which may explain the longer T1 and T2 values in this region. To facilitate comparison with conventional MOLLI and GraSE, T1 and T2 maps were reconstructed for the diastolic cardiac phase. Theoretically, with the proposed framework, T1 and T2 maps can also be reconstructed for any other cardiac phase. Systolic T1 and T2 maps of the subject in Fig. 4 are provided in Supplemental Fig. S3 to demonstrate the feasibility. Systolic T1 and T2 maps may be advantageous in patients suffering from

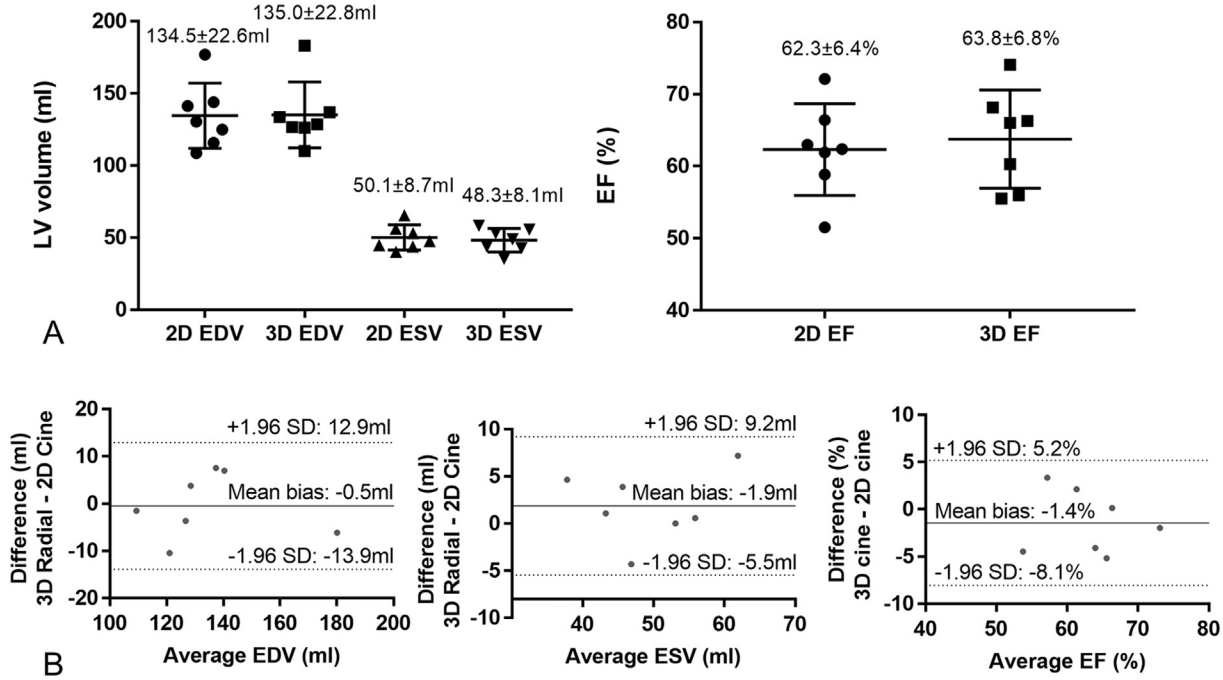

Fig. 10. A: Comparison of EDV (end-diastolic volume), ESV (end-systolic volume), and EF (ejection fraction) between the breath-held, 2D multi-slice cardiac cine imaging and the proposed 3D approach. B: Bland-Altman analyses of EDV, ESV and EF showing the difference between the two methods and the corresponding average. The grey solid line indicates the mean difference, and the grey dotted lines indicate the 95% confidence intervals of limits of agreement.

frequent arrhythmias or heart rate variation, where the onset and duration of the quiescent diastolic resting period is changing, and should also be less prone to partial volume effects from blood due to thicker myocardium at systole [35].

The continuous data acquisition in the free-running sequence provides high scan efficiency and enables cine reconstruction along with the joint T1/T2 mapping. The reconstructed first singular images with the highest SNR were used in this study as cine images. Due to the SPGR readout with low flip angle, the blood-ventricle contrast and the depiction of papillary muscles in the 3D cine images was not as good as in the dedicated breath-hold cine images with bSSFP readout. However, the reconstructed 3D cine images should be enough for measuring cardiac function, providing comparable cardiac function parameters to the breath-hold 2D cine imaging, and for visualizing cardiac wall motion (16-cardiac phase cine images with the proposed technique of one subject are provided in the Supplemental Video). Further validation in patients is warranted before clinical application. Cine images in this study were reconstructed separately for each cardiac phase. However, images from all cardiac phases could be reconstructed simultaneously, e.g., by adding a total variation constraint along the cardiac phase dimension [36]. In this way, redundancy along cardiac phases is exploited which may help to improve the reconstruction quality further although at the expense of increased memory requirement and computational time.

To ensure good quality T1/T2 mapping and cine images, data was acquired for about 11 min. The scan duration was not optimized in this study and shorter acquisition may also be possible. In addition, to resolve cardiac motion, data binning was performed for a given cardiac phase, and the data was not shared between different cardiac phases. However, motion correction of adjacent cardiac phases using the matrix description of general nonrigid motion [37], and/or exploiting redundancy in the motion direction could be investigated in future studies to decrease the total scan time.

In this study, the proposed sequence was evaluated only for native myocardial T1 and T2 mapping, however it should be also applicable to post-contrast mapping. Myocardial T2 is in general not affected by the low concentration contrast, whereas, myocardial T1 is largely shortened after injection of gadolinium-based contrast agents. Therefore, shorter shot interval could be adopted post-contrast due to faster myocardial T1 recovery after IR. If a short interval of 800 ms is used, the scan duration of the proposed sequence could be reduced to about 4 mins. Moreover, faster recovery of longitudinal magnetization after IR leads to higher SNR, which should benefit both T1, T2 mapping and cine reconstruction after contrast injection.

There are several limitations with the proposed technique. Firstly, to address respiratory and cardiac motion, retrospective binning was performed. However, the residual intra-bin respiratory and cardiac motion may cause some image blurring, making the spatial resolution lower than the nominal spatial resolution. Besides, the regularization employed in the HD-PROST reconstruction to reduce the streaking artifacts associated with highly radial undersampling may also influence the effective spatial resolution. Secondly, gridding and re-gridding of the 3D radial data is computationally expensive and time consuming, resulting in long reconstruction time. In future studies, pre-interpolation of the undersampled radial data to Cartesian k-space before iterative reconstruction [38] or GPU implementation of the non-uniform Fourier Transform will be investigated to accelerate the reconstruction process. Lastly, the proposed technique was only validated in healthy subjects to demonstrate the preliminary feasibility. Patients study will be conducted in the next step to test its ability to detect myocardial diseases.

5. Conclusions

In this study, a free-running framework for simultaneous myocardial T1/T2 mapping and cine imaging with 3D whole-heart coverage and isotropic spatial resolution has been proposed. This is the first report describing the acquisition of 3D cine images and co-registered 3D T1 maps and T2 maps in a single free-breathing scan within a feasible scan time. The proposed technique has potential for comprehensive cardiac function evaluation and myocardial tissue characterization.

Supplementary data to this article can be found online at https://doi.org/10.1016/j.mri.2019.08.008.

Funding

This work was supported by the following grants: (1) EPSRC EP/P032311/1, EP/P001009/1 and EP/P007619/1; (2) Wellcome EPSRC Centre for Medical Engineering (NS/A000049/1); (3) the Department of Health via the National Institute for Health Research (NIHR) comprehensive Biomedical Research Centre award to Guy's & St Thomas' NHS Foundation Trust in partnership with King's College London and King's College Hospital NHS Foundation Trust. The views expressed are those of the authors and not necessarily those of the NHS, the NIHR or the Department of Health.

References

[1] Captur G, Manisty C, Moon JC. Cardiac MRI evaluation of myocardial disease. Heart 2016;102(18):1429–35.
[2] Patel AR, Kramer CM. Role of cardiac magnetic resonance in the diagnosis and prognosis of nonischemic cardiomyopathy. JACC Cardiovasc Imaging 2017;10(10):1180–93. Pt A.
[3] Grothues F, Smith GC, Moon JC, Bellenger NG, Collins P, Klein HU, et al. Comparison of interstudy reproducibility of cardiovascular magnetic resonance with two-dimensional echocardiography in normal subjects and in patients with heart failure or left ventricular hypertrophy. Am J Cardiol 2002;90(1):29–34.
[4] Ferreira VM, Piechnik SK, Dall'Armellina E, Karamitsos TD, Francis JM, Choudhury RP, et al. Non-contrast T1-mapping detects acute myocardial edema with high diagnostic accuracy: a comparison to T2-weighted cardiovascular magnetic resonance. J Cardiovasc Magn Reson 2012;14:42.
[5] Bull S, White SK, Piechnik SK, Flett AS, Ferreira VM, Loudon M, et al. Human non-contrast T1 values and correlation with histology in diffuse fibrosis. Heart 2013;99(13):932–7.
[6] Karamitsos TD, Piechnik SK, Banypersad SM, Fontana M, Ntusi NB, Ferreira VM, et al. Noncontrast T1 mapping for the diagnosis of cardiac amyloidosis. JACC Cardiovasc Imaging 2013;6(4):488–97.
[7] Perea RJ, Ortiz-Perez JT, Sole M, Cibeira MT, de Caralt TM, Prat-Gonzalez S, et al. T1 mapping: characterisation of myocardial interstitial space. Insights Imaging 2015;6(2):189–202.
[8] Messroghli DR, Moon JC, Ferreira VM, Grosse-Wortmann L, He T, Kellman P, et al. Clinical recommendations for cardiovascular magnetic resonance mapping of T1, T2, T2* and extracellular volume: a consensus statement by the Society for Cardiovascular Magnetic Resonance (SCMR) endorsed by the European Association for Cardiovascular Imaging (EACVI). J Cardiovasc Magn Reson 2017;19(1):75.
[9] Messroghli DR, Radjenovic A, Kozerke S, Higgins DM, Sivananthan MU, Ridgway JP. Modified Look-Locker inversion recovery (MOLLI) for high-resolution T1 mapping of the heart. Magn Reson Med 2004;52(1):141–6.
[10] Huang TY, Liu YJ, Stemmer A, Poncelet BP. T2 measurement of the human myocardium using a T2-prepared transient-state TrueFISP sequence. Magn Reson Med 2007;57(5):960–6.
[11] Chow K, Flewitt JA, Green JD, Pagano JJ, Friedrich MG, Thompson RB. Saturation recovery single-shot acquisition (SASHA) for myocardial T(1) mapping. Magn Reson Med 2014;71(6):2082–95.
[12] Ding H, Fernandez-de-Manuel L, Schar M, Schuleri KH, Halperin H, He L, et al. Three-dimensional whole-heart T2 mapping at 3T. Magn Reson Med 2015;74(3):803–16.
[13] van Heeswijk RB, Piccini D, Feliciano H, Hullin R, Schwitter J, Stuber M. Self-navigated isotropic three-dimensional cardiac T2 mapping. Magn Reson Med 2015;73(4):1549–54.
[14] Weingartner S, Akcakaya M, Roujol S, Basha T, Stehning C, Kissinger KV, et al. Free-breathing post-contrast three-dimensional T1 mapping: volumetric assessment of myocardial T1 values. Magn Reson Med 2015;73(1):214–22.
[15] Nordio G, Henningsson M, Chiribiri A, Villa ADM, Schneider T, Botnar RM. 3D myocardial T-1 mapping using saturation recovery. J Magn Reson Imaging 2017;46(1):218–27.
[16] Guo R, Chen Z, Wang Y, Herzka DA, Luo J, Ding H. Three-dimensional free breathing whole heart cardiovascular magnetic resonance T1 mapping at 3 T. J Cardiovasc Magn Reson 2018;20(1):64.
[17] Kvernby S, Warntjes MJ, Haraldsson H, Carlhall CJ, Engvall J, Ebbers T. Simultaneous three-dimensional myocardial T1 and T2 mapping in one breath hold with 3D-QALAS. J Cardiovasc Magn Reson 2014;16:102.
[18] Guo R, Chen Z, Herzka DA, Luo J, Ding H. A three-dimensional free-breathing sequence for simultaneous myocardial T1 and T2 mapping. Magn Reson Med 2019;81(2):1031–43.

[19] Weingartner S, Shenoy C, Rieger B, Schad LR, Schulz-Menger J, Akcakaya M. Temporally resolved parametric assessment of Z-magnetization recovery (TOPAZ): dynamic myocardial T1 mapping using a cine steady-state look-locker approach. Magn Reson Med 2018;79(4):2087–100.
[20] Becker KM, Schulz-Menger J, Schaeffter T, Kolbitsch C. Simultaneous high-resolution cardiac T1 mapping and cine imaging using model-based iterative image reconstruction. Magn Reson Med 2019;81(2):1080–91.
[21] Christodoulou AG, Shaw JL, Nguyen C, Yang Q, Xie Y, Wang N, et al. Magnetic resonance multitasking for motion-resolved quantitative cardiovascular imaging. Nat Biomed Eng 2018;2(4):215–26.
[22] Shaw JL, Yang Q, Zhou Z, Deng Z, Nguyen C, Li D, et al. Free-breathing, non-ECG, continuous myocardial T1 mapping with cardiovascular magnetic resonance multitasking. Magn Reson Med 2019;81(4):2450–63.
[23] Qi H, Jaubert O, Bustin A, Cruz G, Chen H, Botnar R, et al. Free-running 3D whole heart myocardial T1 mapping with isotropic spatial resolution. Magn Reson Med 2019;82(4):1331–42. [Epub].
[24] Bustin A, Lima da Cruz G, Jaubert O, Lopez K, Botnar RM, Prieto C. High-dimensionality undersampled patch-based reconstruction (HD-PROST) for accelerated multi-contrast MRI. Magn Reson Med 2019;81(6):3705–19.
[25] Asslander J, Cloos MA, Knoll F, Sodickson DK, Hennig J, Lattanzi R. Low rank alternating direction method of multipliers reconstruction for MR fingerprinting. Magn Reson Med 2018;79(1):83–96.
[26] Sprinkart AM, Luetkens JA, Traber F, Doerner J, Gieseke J, Schnackenburg B, et al. Gradient Spin Echo (GraSE) imaging for fast myocardial T2 mapping. J Cardiovasc Magn Reson 2015;17:12.
[27] Chan RW, Ramsay EA, Cunningham CH, Plewes DB. Temporal stability of adaptive 3D radial MRI using multidimensional golden means. Magn Reson Med 2009;61(2):354–63.
[28] Nezafat R, Stuber M, Ouwerkerk R, Gharib AM, Desai MY, Pettigrew RI. B1-insensitive T2 preparation for improved coronary magnetic resonance angiography at 3 T. Magn Reson Med 2006;55(4):858–64.
[29] Seiberlich N, Breuer F, Blaimer M, Jakob P, Griswold M. Self-calibrating GRAPPA operator gridding for radial and spiral trajectories. Magn Reson Med 2008;59(4):930–5.
[30] Captur G, Gatehouse P, Keenan KE, Heslinga FG, Bruehl R, Prothmann M, et al. A medical device-grade T1 and ECV phantom for global T1 mapping quality assurance-the T1 Mapping and ECV Standardization in cardiovascular magnetic resonance (T1MES) program. J Cardiovasc Magn Reson 2016;18(1):58.
[31] Messroghli DR, Greiser A, Frohlich M, Dietz R, Schulz-Menger J. Optimization and validation of a fully-integrated pulse sequence for modified look-locker inversion-recovery (MOLLI) T1 mapping of the heart. J Magn Reson Imaging 2007;26(4):1081–6.
[32] Bustin A, Cruz G, Jaubert O, Lopez K, Botnar RM, Prieto C. High-dimensionality undersampled patch-based reconstruction (HD-PROST) for accelerated multi-contrast magnetic resonance imaging. Magn Reson Med 2019;81(6):3705–19. [Epub].
[33] Cerqueira MD, Weissman NJ, Dilsizian V, Jacobs AK, Kaul S, Laskey WK, et al. Standardized myocardial segmentation and nomenclature for tomographic imaging of the heart. A statement for healthcare professionals from the Cardiac Imaging Committee of the Council on Clinical Cardiology of the American Heart Association. J Nucl Cardiol 2002;9(2):240–5.
[34] Heiberg E, Sjogren J, Ugander M, Carlsson M, Engblom H, Arheden H. Design and validation of segment–freely available software for cardiovascular image analysis. BMC Med Imaging 2010;10(1).
[35] Ferreira VM, Wijesurendra RS, Liu A, Greiser A, Casadei B, Robson MD, et al. Systolic ShMOLLI myocardial T1-mapping for improved robustness to partial-volume effects and applications in tachyarrhythmias. J Cardiovasc Magn Reson 2015;17:77.
[36] Feng L, Axel L, Chandarana H, Block KT, Sodickson DK, Otazo R. XD-GRASP: golden-angle radial MRI with reconstruction of extra motion-state dimensions using compressed sensing. Magn Reson Med 2016;75(2):775–88.
[37] Batchelor PG, Atkinson D, Irarrazaval P, Hill DL, Hajnal J, Larkman D. Matrix description of general motion correction applied to multishot images. Magn Reson Med 2005;54(5):1273–80.
[38] Benkert T, Tian Y, Huang C, DiBella EVR, Chandarana H, Feng L. Optimization and validation of accelerated golden-angle radial sparse MRI reconstruction with self-calibrating GRAPPA operator gridding. Magn Reson Med 2018;80(1):286–93.